Polarization-gated surface enhanced optical fields for ultrafast electron acceleration

Peifen Lu, Jian Wu[1], Hongxing Qi, and Heping Zeng[2]

State Key Laboratory of Precision Spectroscopy, East China Normal University, Shanghai 200062, China
[1] Corresponding author: jwu@phy.ecnu.edu.cn
[2] Corresponding author: hpzeng@phy.ecnu.edu.cn

Abstract: We show that the field polarization of the surface-plasmon-resonance enhanced optical field can be controlled to be linear with doubled intensity enhancement by using the polarization-gated excitation scheme with two counter-incident femtosecond laser pulses under the Kretschmann configuration, which is hence used for ultrafast electron acceleration to increase the maximum kinetic energy. The spatiotemporal evolution of the polarization-gated surface-enhanced optical field is studied by means of a simplified analytical model to describe the dynamical processes of electron acceleration, the kinetic energy and emission angular distributions of the accelerated electrons.

OCIS codes: (240.6680) Surface plasmons; (320.7110) Ultrafast nonlinear optics

References and links

1. B. Siwick, J. Dwyer, R. Jordan, and R. Miller, "An atomic-level view of melting using femtosecond electron diffraction," Science **302**, 1382-1385 (2003).
2. P. Baum, D. Yang, and A. Zewail, "4D Visualization of Transitional Structures in Phase Transformations by Electrons Diffraction," Science **318**, 788-791 (2007).
3. V. Lobastov, R. Srinivasan, and A. Zewail, "Four-dimensional ultrafast electron microscopy," Proc. Nat. Acad. Sci. **102**, 7069-7073 (2005).
4. P. Baum and A. Zewail, "Attosecond electron pulses for 4D diffraction and microscopy," Proc. Nat. Acad. Sci. **104**, 18409-18414 (2007).
5. M. Schelev, G. Bryukhnevich, V. Lozovoi, M. Monastyrski, A. Prokhorov, A. Smirnov, and N. Vorobiev, "500-fs photoelectron gun for time-resolved electron diffraction experiments," Opt. Eng. **37**, 2249-2254 (1998).
6. H. Park, J. Baskin, O. Kwon, and A. Zewail, "Atomic-Scale Imaging in Real and Energy Space Developed in Ultrafast Electron Microscopy," Nano. Lett. **7**, 2545-2551 (2007).
7. J. Zawadzka, D. Jaroszynski, J. Carey, and K. Wynne, "Evanescent-wave acceleration of ultrafast electron pulses," Appl. Phys. Lett. **79**, 2130-2132 (2001).
8. J. Kupersztych, P. Monchicourt, and M. Raynaud, "Ponderomotive Acceleration of Photoelectrons in Surface-Plasmon-Assisted Multiphoton Emission," Phys. Rev. Lett. **86**, 5180-5183 (2001).
9. S. Irvine, A. Dechant, and A. Elezzabi, "Generation of 0.4-keV Femtosecond Electron Pulses using Impulsively Excited Surface Plasmons," Phys. Rev. Lett. **93**, 184801 (2004).
10. H. Raether, *Surface Plasmons on Smooth and Rough Surfaces and on Gratings* (Springler-Verlag, Berlin, 1988).
11. J. Wu, H. Qi, and H. Zeng, "Extreme-ultraviolet frequency comb generation by polarization-gated surface-enhanced optical fields," Appl. Phys. Lett. **93**, 051103 (2008).
12. P. Lu, J. Wu, H. Qi, and H. Zeng, "Ponderomotive electron acceleration by polarization-gated surface-enhanced optical fields," Appl. Phys. Lett. **93**, 201108 (2008).
13. P. Dombi and P. Rácz, "Ultrafast monoenergetic electron source by optical waveform control of surface plasmons," Opt. Express **16**, 2887-2893 (2008).
14. S. Irvine and A. Elezzabi, "Surface-plasmon-based electron acceleration," Phys. Rev. A **73**, 013815 (2006).
15. B. Siwick, J. Dwyer, R. Jordan, and R. Miller, "Ultrafast electron optics: Propagation dynamics of femtosecond electron packets," J. Appl. Phys. **92**, 1643-1648 (2002).
16. A. Taflove, *Computational Electrodynamics* (Artech House, Boston, 1995).

1. Introduction

Ultrashort electron pulse with ultrahigh spatial and temporal resolutions has been extensively studied for its applications in time-resolved electron diffraction [1,2] and electron microscopy

#105780 - $15.00 USD Received 6 Jan 2009; revised 12 Feb 2009; accepted 13 Feb 2009; published 6 Mar 2009

[3,4] to investigate underlying ultrafast processes in the micro-world. So far, most of the ultrashort energetic electrons are produced by the configuration using a high-voltage DC electric field to accelerate photoelectrons created by intense femtosecond (fs) laser pulses [5,6]. Benefited from the rapid development of fs laser pulses with ultrahigh intensities, more efforts have been made to the optically based generation and acceleration of ultrafast electrons. It has been demonstrated recently that ultrafast electrons with keV kinetic energy could be excited directly by intense fs laser pulse with surface-plasmon-resonance (SPR) enhanced optical field of spatially high-gradient intensity distribution, which firstly liberates electrons from the metal surface through multi-photon ionization process and then accelerates them to high kinetic energies [7-9]. This provides a straightforward all-optical process for simultaneously generation and acceleration of ultrafast electron pulses, which represents the potential for the development of compact optical-pump electron-probe systems. However, the intrinsic elliptically polarized feature [10] of the SPR-enhanced optical field dramatically limits the effective field intensity and thus the finial kinetic energies of accelerated electrons. More recently, it was demonstrated that the polarization of the SPR-enhanced optical field at a certain region close to the metal surface can be controlled to be linear along the normal of the surface by using a polarization-gated excitation scheme [11]. We applied the polarization-gated SPR-enhanced optical field to ultrafast electron acceleration and our numerical results showed that such a polarization-gated SPR-enhanced optical field with a perpendicular linearly polarized mode resulted in an almost doubled maximum kinetic energy as well as a symmetric angular distribution about the favorable forward emission direction as compared with the conventional one-pulse excitation scheme [12]. The purpose of this work is to present the quantitative and general formulation as well as complete elaboration on the polarization control of the SPR-enhanced optical fields and its application in ultrafast electron acceleration by both analytical and simulation procedures.

We focused on the investigation of the detailed spatiotemporal evolution of the polarization-gated SPR-enhanced optical field, proposed a simplified analytical model to describe the dynamical processes of the accelerating electrons and explored the main factors on the kinetic energy and the emission angle during the electron acceleration. The practicability of our simplified analytical model was further proved by the rigorous simulations of finite-difference time-domain (FDTD) method, and the good agreement with the results was found.

2. Simplified description of the enhanced optical field

As presented in Fig. 1, the Kretschmann configuration is considered for the coupling of optical field and surface plasmon (SP) waves. Two p-polarized 20 fs laser pulses at 800 nm with equal intensities are steered to excite SP waves close to the surface of a 50 nm silver film deposited on a prism, which launches SPR at an incident angle of 45°. In order to have an intuitive picture of the polarization-gated excitation scheme under the driving of two synchronized fs laser pulses of p-polarization (fs pulses A and B as labeled in Fig. 1), we firstly consider the simplified formulae [13] for the SPR-enhanced optical field E_{SP} on the vacuum side of the metal film

$$\begin{aligned}
E_{SP,x_A}(x,y,t) &= \beta E(x,t)\cos\left[k_{SP}(x+L/2)-\omega_0 t-\pi/2+\varphi_0\right]e^{-\alpha y}\\
E_{SP,y_A}(x,y,t) &= E(x,t)\cos\left[k_{SP}(x+L/2)-\omega_0 t+\varphi_0\right]e^{-\alpha y}\\
E_{SP,x_B}(x,y,t) &= \beta E(-x,t)\cos\left[-k_{SP}(x-L/2)-\omega_0 t+\pi/2+\varphi_0\right]e^{-\alpha y}\\
E_{SP,y_B}(x,y,t) &= E(-x,t)\cos\left[-k_{SP}(x-L/2)-\omega_0 t+\varphi_0\right]e^{-\alpha y}
\end{aligned}, \qquad (1)$$

where, $E_{SP,x(y)\_A(B)}$ is the $x(y)$ component of the SPR-enhanced optical field excited by the incident laser pulse A (or B), β is the ratio between the amplitudes of the x- and y-components of E_{SP} and determined to be ~0.45 by numerically integrating the Maxwell's equations for the configuration considered in this work, $E(x,t)$ is the envelope function of SPR-enhanced field,

#105780 - $15.00 USD Received 6 Jan 2009; revised 12 Feb 2009; accepted 13 Feb 2009; published 6 Mar 2009

k_{SP} is the wave vector of SP wave, L is the length of the metal film, ω_0 and φ_0 are respectively, the carrier frequency and carrier envelope phase of the optical pulse. By assuming that the spatial beam profile of the incident laser is a constant E_0 and the two synchronized pulses arrive at the center of the metal surface where x=0 at the same time t_0, the envelope function of SPR-enhanced field can be expressed as

$$E(\pm x,t) = E_0 exp\left\{-\left[(t - t_0 \mp k_{SP}x/\omega_0)/\tau_0\right]^2\right\}. \tag{2}$$

Here, τ_0 is the duration of the incident laser pulse. Obviously, it can be derived from Eq. (2) that for the position of x=0, i.e., at the center of the metal surface

$$E(x,t) \equiv E(-x,t) = E(0,t) = E_0 exp\left\{-\left[(t - t_0)/\tau_0\right]^2\right\}. \tag{3}$$

Hence, the SPR-enhanced optical field at the central position excited by these two p-polarized laser pulses can be written as:

$$\begin{aligned} E_{SP,x}(0,0,t) &= E_{SP,x\_A}(0,0,t) + E_{SP,x\_B}(0,0,t) = 0 \\ E_{SP,y}(0,0,t) &= E_{SP,y\_A}(0,0,t) + E_{SP,y\_B}(0,0,t) = 2E(0,t)\cos(k_{SP}L/2 - \omega_0 t) \end{aligned}. \tag{4}$$

This indicates an absolutely linear polarization mode rather than the intrinsic elliptical one and which has no x-component of the electric field, i.e., the SPR-enhanced field is perpendicularly linearly polarized. Meanwhile, it can be derived that the maximum enhanced intensity can be almost doubled as compared with one-pulse excitation scheme for the same total incident intensity. Furthermore, for the positions very close to the center, the identical equation $E(-x,t)\equiv E(x,t)$ can approximately exist owing to the negligible difference between $E(-x,0)$ and $E(x,0)$. So we obtain the enhanced optical field for a small region near the center of the metal surface as:

$$\begin{aligned} E_{SP,x}(x,0,t) &= 2\beta E(0,t)\sin(k_{SP}x)\cos(k_{SP}L/2 - \omega_0 t) \\ E_{SP,y}(x,0,t) &= 2E(0,t)\cos(k_{SP}x)\cos(k_{SP}L/2 - \omega_0 t) \\ E_{SP}(x,0,t) &= \sqrt{E_{SP,x}^2(x,0,t) + E_{SP,y}^2(x,0,t)} \\ &= 2E(0,t)\cos(k_{SP}L/2 - \omega_0 t)\sqrt{\beta^2 + (1-\beta^2)\cos^2(k_{SP}x)} \end{aligned}. \tag{5}$$

According to Eqs. (5), we can clearly see that there is a periodical evolution of the linear polarization direction along the surface with a period of $\lambda_{SP}/2$. Here, $\lambda_{SP}=2\pi/k_{SP}$, which is the wavelength of the SP wave. Meanwhile, as a result of the interference of two counter-propagating SP waves, the maximal and minimal amplitudes of x- and y-components of the electric field emerge along the surface with the same period $\lambda_{SP}/2$ as illustrated in Fig. 2. In fact, $E(x,t)$ is determined by the temporal and spatial beam profiles of the incident pulse. Thus, for the polarization-gated scheme, the modes along the surface away from x=0 gradually deviate from linear polarization toward elliptical polarization as shown in Fig. 3(a). The typical polarization mode of the SPR-enhanced optical field by the conventional one-pulse excitation scheme is shown in Fig. 3(b). In Fig. 4, time-dependent enhanced optical fields of three representative positions on the metal surface (x=0 and $x=\pm 2\lambda_{SP}$) are observed in order to have a quick look at the overall distribution of the enhanced optical field, which also provides a clear view on the formation of the polarization-gated SPR-enhanced optical field. Figures 4(1a)-4(1c) demonstrate that the perpendicularly linearly polarized mode originates from the interference of the two precisely synchronized SP waves, which are respectively excited by incident laser pulses A and B. As shown in Fig. 4(2c) at the position of $x=2\lambda_{SP}$, E_y is firstly $\pi/2$ ahead of E_x while finally E_y is $\pi/2$ behind, which attributes to the earlier arrival of pulse-B than pulse-A. Similarly, as presented in Fig. 4(3c) at the position of $x=-2\lambda_{SP}$, E_x is firstly $\pi/2$ ahead of E_y while finally E_y is $\pi/2$ ahead since pulse-A arrives earlier than pulse-B. So far, the

#105780 - $15.00 USD Received 6 Jan 2009; revised 12 Feb 2009; accepted 13 Feb 2009; published 6 Mar 2009

general features of the polarization-gated SPR-enhanced optical field have been discussed, which response directly to the ponderomotive electron acceleration as will be discussed in what follows.

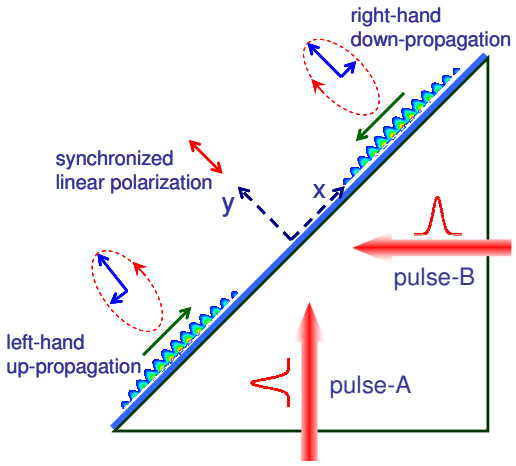

Fig. 1. Ponderomotive electron acceleration scheme based on polarization-gated SPR-enhanced optical field using the Kretschmann configuration.

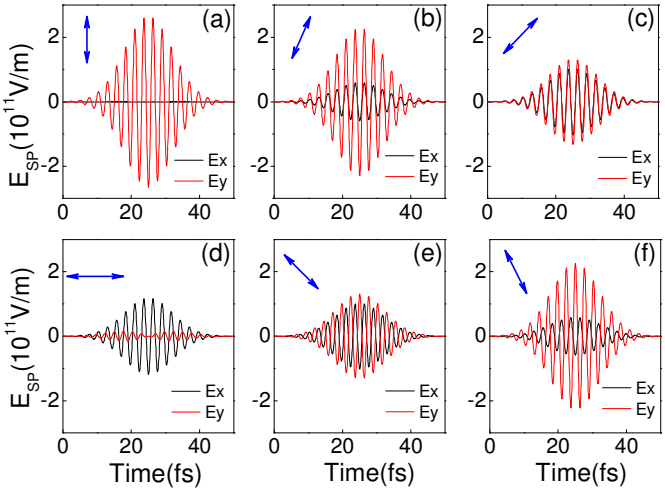

Fig. 2. Time-dependent SPR-enhanced optical field components of six observation positions on the metal surface [according to Eqs. (1)] where (a) x=0, (b) $x=\lambda_{SP}/12$, (c) $x=\lambda_{SP}/6$, (d) $x=\lambda_{SP}/4$, (e) $x=\lambda_{SP}/3$, and (f) $x=5\lambda_{SP}/12$, which indicate the periodical evolution of the enhanced electric field along the metal surface. The arrows in the sub-Figs. indicate the polarization directions.

#105780 - $15.00 USD Received 6 Jan 2009; revised 12 Feb 2009; accepted 13 Feb 2009; published 6 Mar 2009

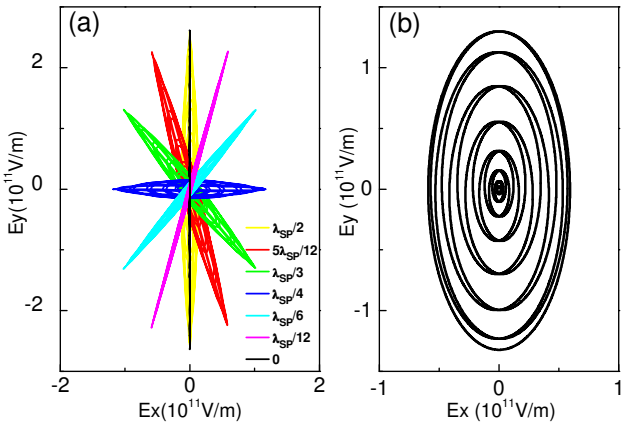

Fig. 3. (a). The polarization direction evolution of the enhanced optical field near the surface center with a period ranging from x=0 to x=λ_{SP}/2 using polarization-gated excitation scheme [according to Eqs. (1)]. Different colors stand for the different positions along the metal surface. (b). The polarization of the enhanced optical field using conventional one-pulse excitation scheme. The evolutions in (a) and (b) are observed within a time period ranged from -25 to 25 fs, where time zero indicates the envelope peak of the SPR-enhanced optical field.

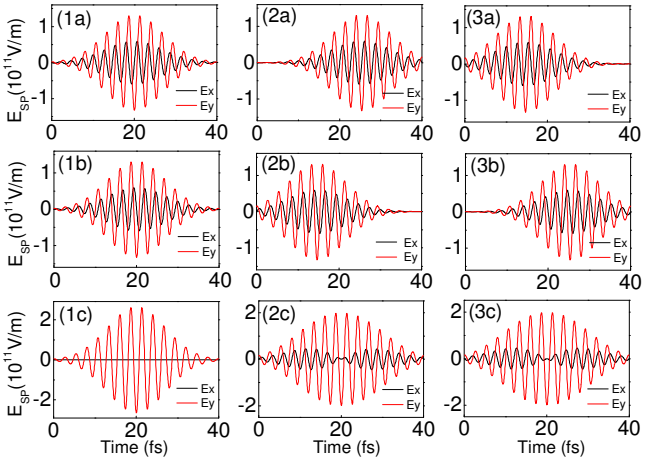

Fig. 4. Superposition of the SPR-enhanced optical fields induced by incident pulse-A and pulse-B [according to Eqs. (1)] respectively at three observation positions along the metal surface of (1a) ~ (1c) x=0, (2a) ~ (2c) x=2λ_{SP}, and (3a) ~ (3c) x=-2λ_{SP}. Rows (a), (b) and (c) represent the SPR-enhanced optical fields respectively induced by incident pulse of pulse-A, pulse-B, and two synchronized pulses as shown in Fig. 1.

3. Simplified description of the electron acceleration

In this section, we study the dynamics of the pondermotive electron acceleration by the SPR-enhanced optical field based on a simplified analytical method. In our calculations, an intensity-dependent three-photon photoemission [14] is considered as an ionization mode to predict the rate at which electrons are generated and the electrons are assumed to have an initial kinetic energy of zero as they are librated from the metal surface. Since it only takes several tens fs for the electrons to fully accelerate to their final kinetic energies within a sub-wavelength spatial region, as shown in Figs. 5(a) and 5(c), the space charge effect [15] is ignored in our model. In addition, as shown in Fig. 6, the temporal interval for generation of electrons that can be accelerated is about 1/4 of every optical cycle since the y-component displacements of the electrons excited by the rest of the optical cycle would be negative, which means the electrons return to the metal-vacuum boundary during their subsequent

#105780 - $15.00 USD Received 6 Jan 2009; revised 12 Feb 2009; accepted 13 Feb 2009; published 6 Mar 2009

acceleration and hence are not included in our following discussions. Once an electron is emitted from the metal surface, it is accelerated by the high-gradient optical field and its motion is governed by the Lorentz force equation. Here, allowing for the fact that the magnetic field close to the metal surface has little effect on the electron acceleration, a simplified equation $d\boldsymbol{v}/dt=-q\boldsymbol{E}/m_e$ is used to approximately describe the electron acceleration, where q/m_e is the charge-to-mass ratio and $\boldsymbol{v}$ is the velocity of the electron.

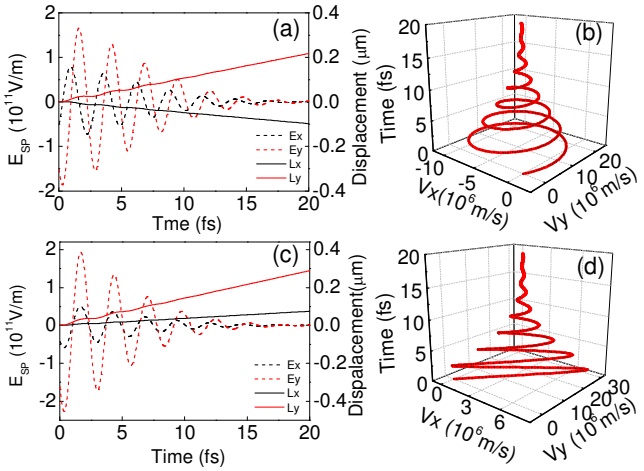

Fig. 5. (a) and (c) The displacement ($L_{x,y}$) and electric field ($E_{x,y}$) components experienced by the test electrons during the ponderomotive acceleration [according to Eqs. (1)], and (b) and (d) the velocity ($V_{x,y}$) components of the electrons accelerated by SPR-enhanced polarization-gated excitation scheme and conventional one-pulse excitation scheme, respectively.

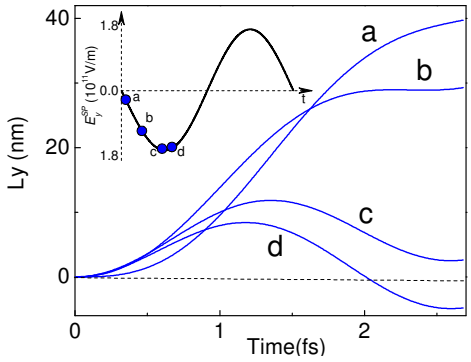

Fig. 6. Y-component displacements of the electrons ejected from the metal surface at different instances of an optical cycle with various phases of E_y [according to Eqs. (9) or Eqs. (14)]. Curves a, b, c, and d, respectively, represent the y-component displacements of the electrons within an optical cycle acceleration after being ejected from corresponding instances a, b, c, d as labeled in the inset.

By using Eqs. (1), we obtain the numerical results as illustrated in Figs. 5(b) and 5(d), which present the processes of the electron kinetic energy gains in the presence of the ponderomotive potential of the SPR-enhanced optical fields respectively created by one-pulse excitation and polarization-gated excitation schemes. It seems that for both of these two excitation schemes, an electron reaches its stable kinetic energy in a form analogous to damped vibration. Hence, we can make an approximation that the final kinetic energy of an accelerated electron can be estimated by the average of maximum and minimum values of its velocity during the first optical cycle. Meanwhile, Figs. 5(a) and (b) indicate that the electron

#105780 - $15.00 USD Received 6 Jan 2009; revised 12 Feb 2009; accepted 13 Feb 2009; published 6 Mar 2009

emission angle θ can be characterized by the expression $\tan\theta=L_y/L_x$, where L_x and L_y are the x- and y-component displacements of an electron, respectively. Due to the fact that in the first optical cycle the displacements of the electron is quite small and the envelope function of SPR-enhanced field can be treated as a constant E_0, the electric field experienced by the accelerated electrons can be approximately written as:

$$\begin{aligned} E_x(x,y,t) &= \beta E_0 \ sin(\omega_0 t + \varphi + \delta\varphi) \\ E_y(x,y,t) &= E_0 sin(\omega_0 t + \varphi) \end{aligned} \quad . \tag{6}$$

Here, φ is the phase of E_y when the electron is ejected from the metal surface and $\delta\varphi$ is the phase difference between E_x and E_y. In the following, we will investigate the dependences of the kinetic energy and emission angle of an accelerated electron by observing its motion in the first optical cycle accelerating based on the above-mentioned approximation.

For the case of one-pulse excitation scheme, $\delta\varphi=\pi/2$. So we have the electric field experienced by an accelerating electron in the first optical cycle after its ionization as:

$$\begin{aligned} E_x(x,y,t) &= \beta E_0 \ sin(\omega_0 t + \varphi + \pi/2) \\ E_y(x,y,t) &= E_0 sin(\omega_0 t + \varphi) \end{aligned} \quad . \tag{7}$$

Here, $t\in [0,2\pi/\omega_0]$ since we only observe the motion of an accelerating electron in the first optical cycle after its ionization and $\varphi\in [\pi,3\pi/2]$ for the electron generation interval. Employing the equation $d\boldsymbol{v}/dt=-q\boldsymbol{E}/m_e$ with the initial conditions $v_x(0)=0$ and $v_y(0)=0$, we obtain the velocity components of the accelerating electron:

$$\begin{aligned} v_x(t) &= \int_0^t \frac{-qE_x}{m_e} dt = \frac{-q\beta E_0}{m_e\omega_0}\left[\sin(\omega_0 t+\varphi) - \sin\varphi\right] \\ v_y(t) &= \int_0^t \frac{-qE_y}{m_e} dt = \frac{-qE_0}{m_e\omega_0}\left[-\cos(\omega_0 t+\varphi) + \cos\varphi\right] \end{aligned} \quad . \tag{8}$$

Then employing $L_x(0)=0$ and $L_y(0)=0$, we get the displacement components of the accelerating electron after an optical cycle:

$$\begin{aligned} L_x &= \int_0^{2\pi/\omega_0} v_x dt = \frac{2\pi q\beta E_0}{m_e\omega_0^2}\sin\varphi \\ L_y &= \int_0^{2\pi/\omega_0} v_y dt = \frac{-2\pi qE_0}{m_e\omega_0^2}\cos\varphi \end{aligned} \quad . \tag{9}$$

Hence, we can estimate the final kinetic energy and emission angle of the electron respectively by

$$\begin{aligned} E_k &= \frac{1}{2}m_e\left(\left[\frac{(v_x)_{\max}+(v_x)_{\min}}{2}\right]^2 + \left[\frac{(v_y)_{\max}+(v_y)_{\min}}{2}\right]^2\right) \\ &= \frac{q^2E_0^2}{2m_e\omega_0^2}\left[1+(\beta^2-1)\sin^2\varphi\right] \end{aligned} , \tag{10}$$

and

$$\tan\theta = \frac{L_y}{L_x} = \frac{1}{-\beta\tan\varphi} \ . \tag{11}$$

According to Eqs. (10) and (11), we can derive that the final kinetic energy and emission angle of the accelerated electron only depend on φ since here β is a constant. As a

#105780 - $15.00 USD Received 6 Jan 2009; revised 12 Feb 2009; accepted 13 Feb 2009; published 6 Mar 2009

consequence, electrons emitted at different instants of an optical cycle have different final kinetic energies and different emission angles. Furthermore, it can be derived that $\tan\theta<0$ as $\varphi\in[\pi, 3\pi/2]$, which results in an angular distribution ranging from 90° to 180°. All the above derivations are provided to be a reasonable approximation for their quite good agreement with the numerical results shown in Fig. 7. As presented in Fig. 7, electrons ejected from the instances with same phase of E_y labeled as points 1, 2, 3, and 4 accelerate almost along a certain direction, as illustrated by the corresponding colored trajectory lines 1, 2, 3, and 4, respectively; whereas electrons ejected at the instances with different phases of E_y labeled as points 1, 5, 6, 7, and 8 emitted at various directions, as illustrated by the corresponding black trajectory lines 1, 5, 6, 7 and 8, respectively.

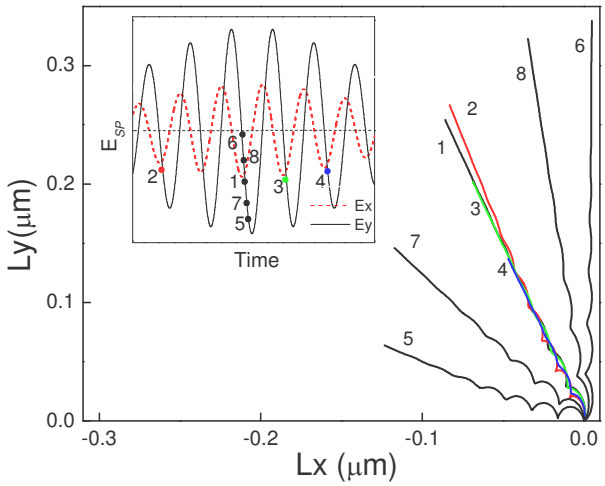

Fig. 7. Calculated trajectories of the electrons corresponding to the excitation instances labeled in the inset [according to Eqs. (7) and Eqs. (9)], in which points 1, 5, 6, 7, and 8 stand for the instances in the same optical cycle with various phases of E_y, while points 1, 2, 3, and 4 stand for the instances in different optical cycles with same phase of E_y.

For the case of polarization-gated excitation scheme, $\delta\varphi=0$ or π. So we obtain the electric field experienced by an accelerating electron in the first optical cycle after its ionization:

$$\begin{aligned} E_x(x,y,t) &= \pm\beta(x)E_0\ sin(\omega_0 t+\varphi) \\ E_y(x,y,t) &= E_0 sin(\omega_0 t+\varphi) \end{aligned} \quad . \tag{12}$$

Here, $\beta(x)=\beta\tan(k_{SP}x)$ is a function of position x with a period of π/k_{SP}, which can be derived from Eqs. (5) due to the modulated optical intensity along the metal surface as a result of the interference of the two counter-propagating SPR-enhanced optical waves. And as the same conditions in one-pulse excitation scheme, there are $t\in[0,2\pi/\omega_0]$ and $\varphi\in[\pi,3\pi/2]$. Employing the equation $d\boldsymbol{v}/dt=-q\boldsymbol{E}/m_e$ with the initial conditions $v_x(0)=0$ and $v_y(0)=0$, we obtain the velocity components of the accelerating electron:

$$\begin{aligned} v_x(t) &= \int_0^t \frac{-qE_x}{m_e}dt = \mp\frac{q\beta(x)E_0}{m_e\omega_0}\left[-\cos(\omega_0 t+\varphi)+\cos\varphi\right] \\ v_y(t) &= \int_0^t \frac{-qE_y}{m_e}dt = \frac{-qE_0}{m_e\omega_0}\left[-\cos(\omega_0 t+\varphi)+\cos\varphi\right] \end{aligned} \quad . \tag{13}$$

Then employing the initial conditions $L_x(0)=0$ and $L_y(0)=0$, we get the displacement components of the accelerating electron after an optical cycle:

#105780 - $15.00 USD Received 6 Jan 2009; revised 12 Feb 2009; accepted 13 Feb 2009; published 6 Mar 2009

$$L_x = \int_0^{2\pi/\omega_0} v_x dt = \frac{\mp 2\pi q \beta(x) E_0}{m_e \omega_0^2} \cos\varphi$$
$$L_y = \int_0^{2\pi/\omega_0} v_y dt = \frac{-2\pi q E_0}{m_e \omega_0^2} \cos\varphi \quad . \tag{14}$$

Hence, we can estimate the final kinetic energy and emission angle of the electron respectively by

$$E_k = \frac{1}{2} m_e \left\{ \left[\frac{(v_x)_{\max} + (v_x)_{\min}}{2} \right]^2 + \left[\frac{(v_y)_{\max} + (v_y)_{\min}}{2} \right]^2 \right\} = \frac{\left[\beta^2(x) + 1\right] q^2 E_0^2 \cos^2\varphi}{2 m_e \omega_0^2} , \tag{15}$$

and

$$\tan\theta = \frac{L_y}{L_x} = \pm \frac{1}{\beta(x)} \quad . \tag{16}$$

It can be seen from Eqs. (15) and (16) that the final kinetic energy depends on φ and $\beta(x)$, while the emission angle only depends on $\beta(x)$. Consequently, electrons ejected from different instances and positions have quite different final kinetic energies. Meanwhile, mainly determined by $\beta(x)$, electrons from a certain position emit concentratively along a certain direction; however, those from various positions have various emission angles. Furthermore, it can be derived that $\tan\theta \in [-\infty, \infty]$ as $\beta(x) \in [-\infty, \infty]$, which leads to a symmetric angular distribution ranging from 0° to 180°. All the above conclusions are confirmed by the numerical results without approximations as illustrated in Fig. 8. In Fig. 8(a), the different polarization directions of the enhanced optical field mean different values of $\beta(x)$ on the five observation positions labeled by 1, 2, 3, 4, and 5. And the trajectories of electrons ejected from corresponding positions are illustrated with the same labeled numbers as shown in Fig. 8(b).

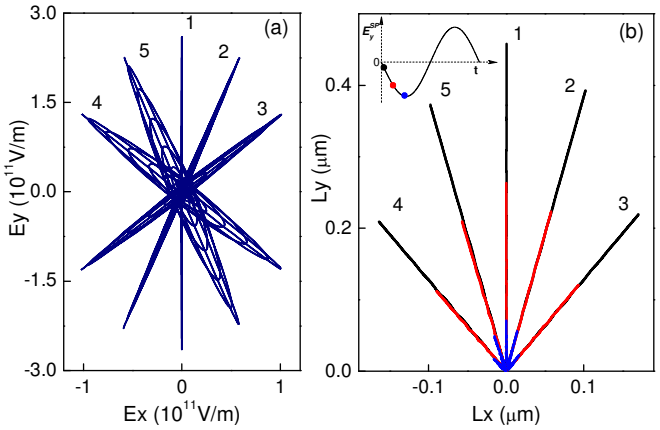

Fig. 8. (a) Polarizations of the enhanced optical fields at five observation positions along the metal surface. (b) Trajectories of electrons emitted from corresponding positions at three different instances as marked in the inset [according to Eqs. (12) and Eqs. (14)]. Line groups 1, 2, 3, 4, and 5 stand for the electrons emitted from five different positions as x=0, x=λ_{SP}/12, x=λ_{SP}/6, x=λ_{SP}/3, and x=5λ_{SP}/12, respectively. In each line group, the black, red and blue lines stand for electrons emitted from three different instances during an optical cycle as indicated in the inset of (b).

#105780 - $15.00 USD Received 6 Jan 2009; revised 12 Feb 2009; accepted 13 Feb 2009; published 6 Mar 2009

4. Simulation based on the finite-difference time-domain method

In the following simulations, we use FDTD method [16] to explore the full distribution of the SPR-enhanced polarization-gated optical field and thus the kinetic energy and emission angular distributions of the accelerated electrons. The Kretschmann configuration once again is employed for optical field coupling, and the Maxwell equations governing the full evolution and distribution of the enhanced optical field are solved numerically by FDTD method with perfect matching layers. Numerical results show that a peak intensity enhancement factor of 80 (or equivalent 40 relative to the sum incident intensity of the two incident pulses) can be achieved by using the polarization-gated scheme, which is almost doubled as compared with the conventional one-pulse incident case with an enhancement factor of 22 for the case considered here. Numerous test electrons are placed uniformly along the metal film in space and all the temporal contributions for intensities larger than 10% of the pulse peak are included (the electrons excited by the rest fields are negligible for their fairly low energies and observation probabilities) in order to represent all the possible trajectories of the accelerated electrons. A relative weight proportional to $I^3(x,y,t)$ is assigned to each accelerated electron by considering the electron emission as a third-order multi-photon process [14], where $I(x,y,t)$ stands for the intensity of the SPR-enhanced optical field. In addition, as mentioned above, the motions of the electrons are governed by Lorentz force equation and neither the secondary electron emission nor space-charge is considered in our calculations.

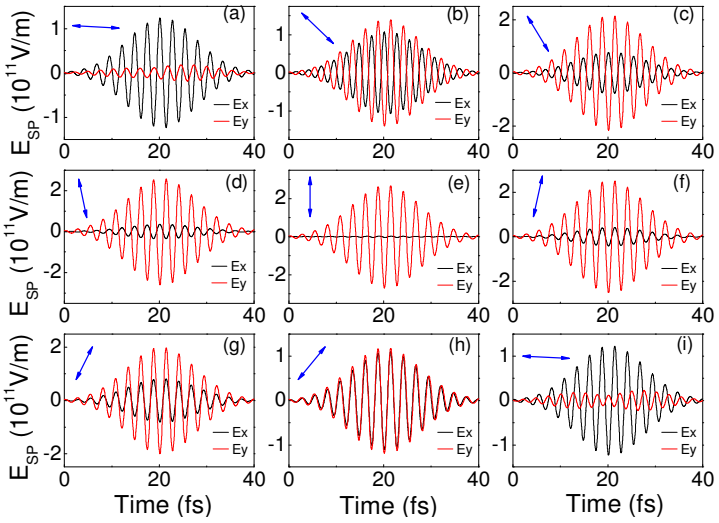

Fig. 9. Evolutions of the SPR-enhanced polarization-gated optical fields at nine observation positions along the metal surface where (a) $x=-\lambda_{SP}/4$, (b) $x=-3\lambda_{SP}/16$, (c) $x=-\lambda_{SP}/8$, (d) $x=-\lambda_{SP}/16$, (e) $x=0$, (f) $x=\lambda_{SP}/16$, (g) $x=\lambda_{SP}/8$, (h) $x=3\lambda_{SP}/16$, and (i) $x=\lambda_{SP}/4$ based on FDTD simulations.

Figure 9 provides information concerning the properties of the SPR-enhanced optical field excited by our polarization-gated scheme. By comparing Fig. 9 with Fig. 2, it can be seen that there is a quite good agreement between the numerical results respectively based on rigorous FDTD method and the previous simplified analytical formulae. Figure 9(e) represents electric field components of a point almost at the centre of the metal surface. Obviously, this indicates a perpendicularly linearly polarized mode with maximum y-component and nearly zero x-component of the enhanced optical field, which attributes to the precise synchronization of the two counter-propagating pulses at the position as what has been illustrated in Fig. 2(a). Furthermore, Figs. 9(a) and 9(i) show that electric polarization modes of the positions away from the center tend to depart from linearly polarization to elliptical polarization. This is due to the break of the synchronization between the two incident pulses at those positions since

#105780 - $15.00 USD Received 6 Jan 2009; revised 12 Feb 2009; accepted 13 Feb 2009; published 6 Mar 2009

pulse-A arrives earlier than pulse-B at positions where $x<0$ while pulse-B arrives earlier at those where $x>0$.

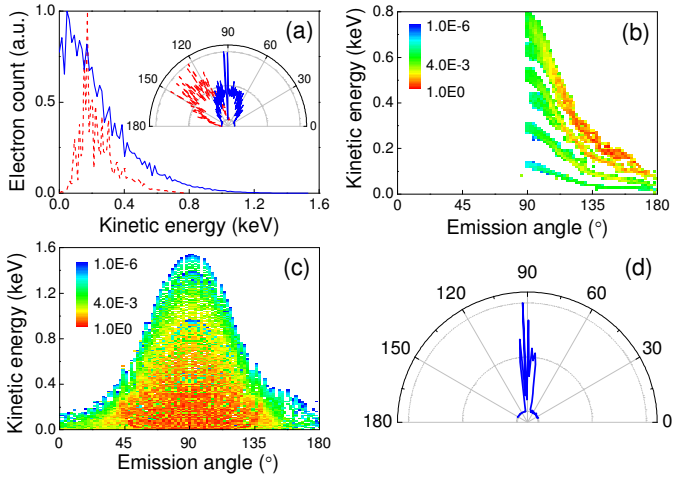

Fig. 10. (a). The kinetic energy spectra and angular distributions (in the inset) of emitted electrons. The red and blue curves stand for the results by using one-pulse excitation scheme with a maximum E_I of 0.4×10^{11} V/m (E_{SP}~1.87×10^{11}V/m), and polarization-gated scheme with a maximum E_I of 0.28×10^{11}V/m for each incident fs laser pulse (E_{SP}~2.63×10^{11}V/m), respectively. (b) and (c) respectively represent the angle-resolved kinetic energy distributions of the electrons accelerated by SPR-enhanced optical field using one-pulse excitation scheme and polarization-gated scheme, where the false color stands for the observation probability. (d) Improved emission angular distribution by coating the prism surface with a quite narrow metal film of 30 nanometers in size (based on FDTD simulations).

In order to have an overall view on the characteristics of electron emission, we also study the kinetic energy spectra, emission angular distribution and angle-resolved kinetic angular distribution. Figure 10(a) provides us a picture of kinetic energy and angular distributions of the accelerated electrons produced by one-pulse excitation and polarization-gated schemes, respectively. As we have discussed previously that there is a strong association between the final kinetic energy and the emission instance in an optical cycle. Both the kinetic energy distributions of these two excitation schemes have broad spectra and the higher the kinetic energy the lower the emission probability is. The insets in Fig. 10(a) present the angular distributions by two different excitation schemes, which consist with the results predicted by Eqs. (11) and (16). It can be seen obviously that the maximum kinetic energy of the accelerated electrons is almost doubled by polarization-gated scheme as compared with one-pulse excitation scheme, which agrees well with our simplified analytical model basing on the doubled peak intensity of the SPR-enhanced field of Eqs. (5). The doubled maximum kinetic energies respectively equal to 1.47 keV for the simplified analytical method and 1.6 keV for the FDTD method, and the slight difference is mainly introduced by the necessary approximation in our simplified analytical model. The sources of the emitted electrons with different kinetic energies can be seen more clearly by taking the angle-resolved kinetic energy distributions as shown in Figs. 10(b) and 10(c), which describe the relationship of emission angle, kinetic energy and emission probability. For one-pulse excitation scheme, as shown in Fig. 10(b), the number of distinct structures on the angle-resolved kinetic energy distribution roughly reveals the number of optical cycles when electrons are generated; whereas the electrons ejected from different positions at the same instance distribute concentratedly due to the fact that optical fields at the observed region have no obvious difference. However, for polarization-gated excitation scheme, the enhanced optical field is quite different from that excited by one-pulse excitation scheme, which attributes to the interference between the two counter-propagating SP waves. Consequently, the gated optical field with polarization

#105780 - $15.00 USD Received 6 Jan 2009; revised 12 Feb 2009; accepted 13 Feb 2009; published 6 Mar 2009

perpendicular to the metal film creates electrons with a large range of kinetic energy distribution and an almost doubled maximum, which shows a normal emission direction. The enhanced optical fields at various positions along the surface with different polarization modes lead to electron emission with relatively low kinetic energies at the corresponding angles. So, as shown in Fig. 10(c), this results in a symmetric emission angular distribution with a preferred forward emission direction but no distinct structures. Furthermore, by using particular surface morphology of the metal film (for example, by depositing a dielectric layer on the metal surface with a suitably wide opening or coating the prism surface with a quite narrow metal film, where only the perpendicularly linear polarization mode is excited), it is possible to produce an ultrafast electron pulse with a quite narrow emission angular distribution of several degrees in the forward direction, as shown in Fig. 10(d).

5. Conclusion

We proposed an electron generation and acceleration scheme based on polarization-gated SPR-enhanced optical field. By using two methods, simplified analytical model and rigorous FDTD solution to Maxwell's equations, we explored the fully spatiotemporal evolution and distribution of the optical field close to the metal surface, and then the detailed dynamics of the electron acceleration, especially the dependences of the final kinetic energy and emission angle of an accelerated electron on the SPR-enhanced optical fields. In comparison with the conventional one-pulse excitation scheme, our numerical results show that the maximum kinetic energy of the accelerated electrons is almost doubled as well as an improved emission angular distribution for our polarization-gated excitation. The polarization-gated scheme provides us an efficient way to control the polarization state of the surface-enhanced optical field, which meanwhile doubles the intensity enhancement. In addition to the ultrafast electron acceleration and XUV frequency comb generation, it can be widely used as a versatile method to investigate many other polarization sensitive processes, such as polarization-dependent nonlinear microscopy, atomic/molecular dynamics under SPR-enhanced field excitation, molecular alignments nearby metal surfaces, and so forth. Promising applications in various fields are thus expected.

Acknowledgments

This work was funded in part by National Natural Science Fund (Grants 10525416 and 10804032), National Key Project for Basic Research (Grant 2006CB806005), Projects from Shanghai Science and Technology Commission (Grants 06JC14025 and 08ZR1407100), Program for Changjiang Scholars and Innovative Research Team in University, and Shanghai Educational Development Foundation (Grant 2008CG29).

#105780 - $15.00 USD Received 6 Jan 2009; revised 12 Feb 2009; accepted 13 Feb 2009; published 6 Mar 2009